Wavefront Measurements of High-Power UV Lasers with a Hartmann Sensor

Emily Armstrong
Our Lady of Mercy High School
LLE Advisors: Matthew Barczys, Brian Kruschwitz

Laboratory for Laser Energetics
University of Rochester
Summer High School Research Program
2012

1. Abstract

Experiments were conducted to determine the effectiveness of the Hartmann sensor as a wavefront diagnostic on the UV portions of the OMEGA EP laser system. Programs in MATLAB were used to model Hartmann grid patterns and then reconstruct wavefronts from grid images. Simulations were run to design basic Hartmann grids for a laboratory proof-of-concept setup with a 532 nm visible laser. Sensor masks were then tested in a series of experimental trials to determine the accuracy of a basic Hartmann sensor. Models of the experimental system were created in OSLO, a commercial ray-tracing program, and compared to the gathered data to verify the reconstruction results. A commercial wavefront sensor was also added to the experimental set-up to provide further confirmation of the Hartmann sensor reconstructions. The concept was proven that the Hartmann sensor would be an effective method for optional wavefront analysis on UV beams entering the OMEGA EP target chamber as well as on the fourth harmonic probe beam, operating at 263 nm, used for diagnostics.

2. Introduction

Wavefront sensing is crucial on large laser systems such as OMEGA EP [1]. An accurate wavefront measurement gives information on whether or not the beam is collimated. If the beam is not collimated, it may not focus at the desired location, such as at the center of the OMEGA EP target chamber. Small scale aberrations indicative of damage, misalignment, or manufacturing errors in the optics of the system are also visible on wavefront measurements. In cases when minimal wavefront aberration is desired, it is valuable to have a measurement of the laser wavefront to help diagnose the optical system.

The Hartmann sensor is an example of a relatively simple technique for determining wavefronts known as a screen test [2]. As shown in figure 1, the sensor itself is a grid of apertures through which the beam passes, blocking sections of the original beam. The beam sections passing through the sensor then land on the light sensor of a camera, forming a spot pattern. Using a beam that is close to perfectly collimated, a reference spot pattern is created for a given sensor. By comparing the reference pattern to the pattern made by the test beam, the slope of the wavefront can be determined at each point that passed through an aperture.

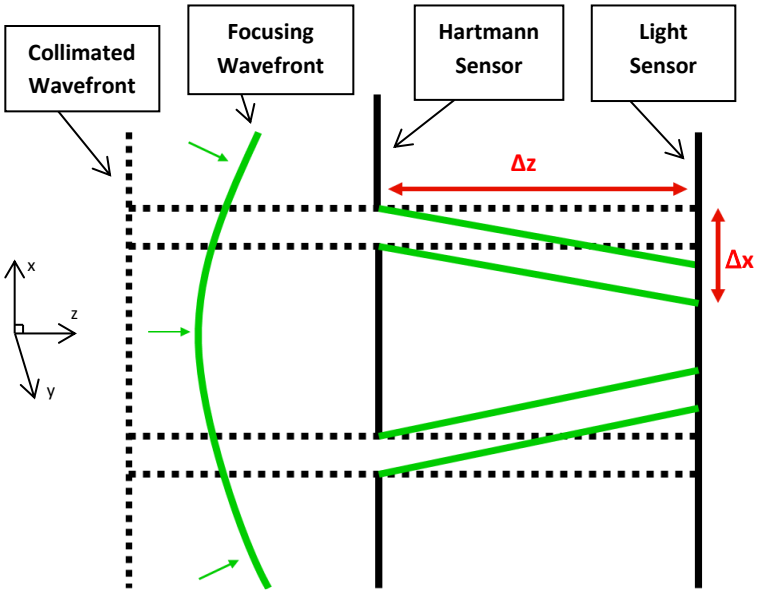

Figure 1: Hartmann Sensor Diagram
This diagram shows the path of a collimated wavefront passing through a Hartmann sensor in dotted lines and a focusing wavefront passing through the same sensor in green. The distance between the mask and the screen is shown as Δz and the distance between the spot made by the collimated beam and that made by the focusing beam is shown as Δx. Using these two distances, the direction of the beamlet through the top aperture can be determined. This direction is perpendicular to the wavefront passing through the aperture.

To determine the direction of a given beamlet, the camera is used to measure the distance between the reference spot of a given aperture and the spot created by the test beam. The beamlet slope in figure 1 is equal to the distance between the spots (Δx) divided by the distance from the mask to the camera (Δz). By using a Hartmann sensor with many apertures, equations are obtained for the variations in height of the wavefront h(x,y) with respect to x and y:

$$\frac{\partial h}{\partial x} = \frac{\Delta x}{\Delta z} \tag{1}$$

$$\frac{\partial h}{\partial y} = \frac{\Delta y}{\Delta z} \tag{2}$$

where $\partial h/\partial x$ and $\partial h/\partial y$ are components of the slope and Δx and Δy are distances that a spot moves from its reference position. These equations model the local wavefront slopes over the entire section of the beam that passes through the sensor. Integrating these slope equations over the space the sensor occupies gives a reconstruction of the actual wavefront incident on the Hartmann sensor in the form h(x,y).

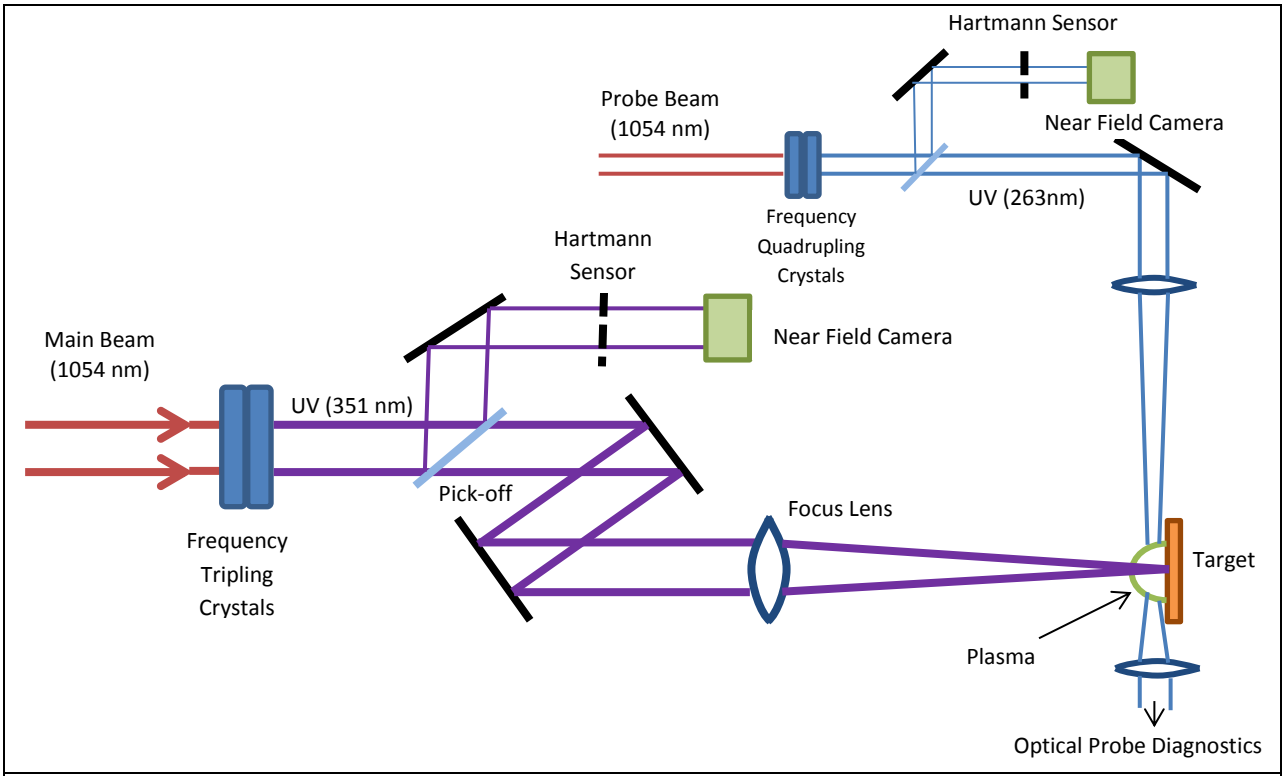

Figure 2: OMEGA EP Diagram – This simplified schematic shows the relevant major portions of the OMEGA EP laser system. Places for proposed Hartmann sensor implementation are depicted.

Portions of the OMEGA EP laser system relevant to the implementation of a Hartmann sensor are shown above in figure 2. The main beams come from a source operating at 1054 nm.

They are amplified at this wavelength, and then pass through the frequency tripling crystals, which shift them to 351 nm. They are then brought to focus on a target, and a plasma is created. A smaller beam, the 1054 nm probe beam, passes through frequency quadrupling crystals and its resultant wavelength is 263 nm. This beam is used to image plasmas created during laser shots with an interferometry technique. Samples of both the probe beam and the main beams can be taken using pick-offs, and their wavefronts can be diagnosed using Hartmann sensors.

The Hartmann sensor was selected as the best method for use with the UV beams on the OMEGA EP laser system for several reasons. First, it is compatible with the system because the sensor masks have no refractive elements, and can therefore be used interchangeably with UV lasers of both wavelengths. In addition, the Hartmann sensor supports use with other wavelengths since the apertures are designed to be large enough to minimize diffractive effects, which would cause interference and blur the spot pattern. Most importantly, the Hartmann sensor mask can be manufactured inexpensively and easily inserted into the existing laser diagnostics on the OMEGA EP system. A Hartmann sensor mask could simply be placed in front of the near field cameras on laser shots for which a wavefront measurement is desired.

The implementation of Hartmann sensors on the OMEGA EP laser would be valuable for several purposes. One use for a Hartmann sensor would be to determine the wavefront of the fourth harmonic probe beam [3] as it enters the OMEGA EP target chamber. Images of the plasma taken using this beam are altered if the wavefront of the probe beam is aberrated. It would be useful to know the wavefront of the beam before it is passed through the plasma to be able to account for this error. A second use for the Hartmann sensor would be to gain an

estimate of the final wavefront on the main UV beamlines (351 nm wavelength). This would give a clearer picture of the aberration introduced to the beams by the optics that transport them from the final measurement point in the infrared sections to the frequency tripling crystals. After the crystals, the beams operate in the UV, and currently there is no way to measure the beamline wavefront. In the future, Hartmann sensors might also be used to determine the exact paths of the focusing beams approaching target chamber center and the area the beams cover on the final optics before entering the target chamber, which can in turn be used to calculate the energy intensity on those optics. Currently, this energy intensity is unknown, and a highest plausible intensity must be assumed in order to avoid damaging the optics. This is a current limiting factor on the energy output of the system, and an accurate wavefront measurement could allow an increase in the total energy output of OMEGA EP.

In this work, a Hartmann sensor was designed to fulfill the need for wavefront sensing in the UV portions of the OMEGA EP laser system. Both the mask itself and the wavefront reconstruction software were tested in an experimental test system. The results from the tested Hartmann sensor were compared to wavefront measurements from a Shack-Hartmann sensor, and found to be accurate. These results affirm the effectiveness of the Hartmann sensor, providing a proof-of-concept for implementing the technique on OMEGA EP.

3. Experimental Set-up

The Hartmann sensor was tested in a small-scale optical system. Figure 3 shows a schematic diagram of the experimental set-up. The laser used for the tests was a 5 milli-watt beam operating at 532 nm, 1 mm in diameter.

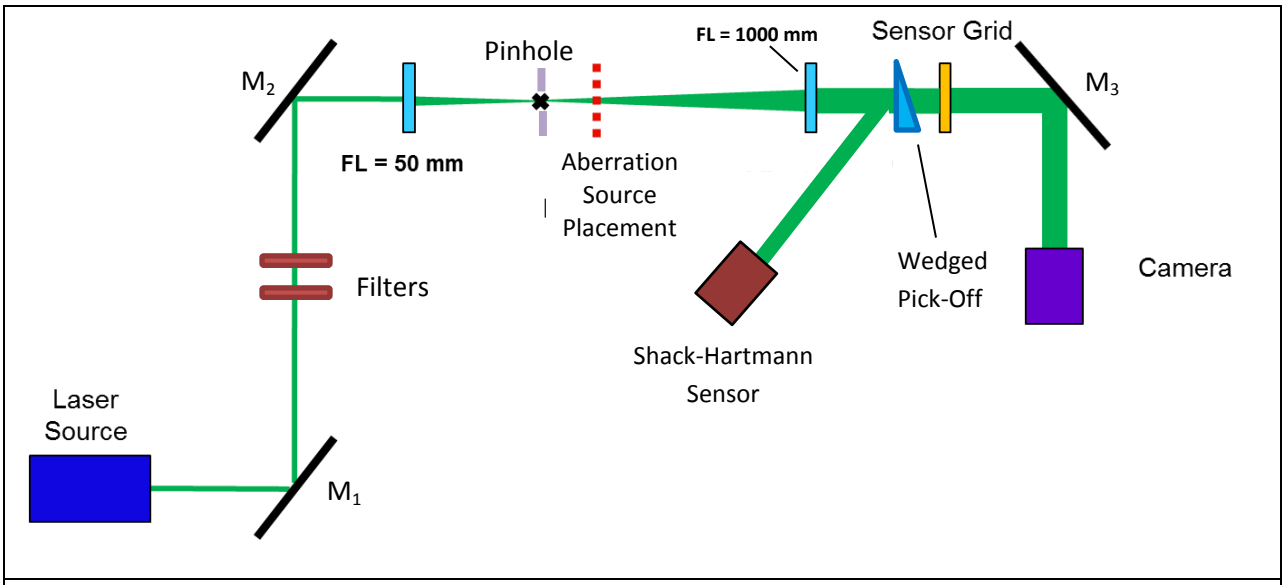

Figure 3: Optical System Diagram – This is a simplified depiction of the optical set-up used to test the Hartmann sensors. Black lines represent mirrors and the black X indicates where the beam comes to focus in the telescope system.

The mirrors M_1 and M_2 are used to precisely position and point the beam. In between these mirrors is a pair of filters to decrease the intensity of the beam and avoid damaging the sensitive light sensor in the camera. A beam expander is used to increase the diameter of the laser in order to fill the approximately 11 mm diameter of the sensor grid. A 50 mm focal length plano-convex lens made of fused silica is used to bring the beam to focus through a pinhole. This has a diameter of 100 µm and blocks light that is not focusing in the desired path in order to smooth the spatial intensity profile of the laser beam. Then, when the beam radius has increased by a factor of 20, a 1000 mm focal length lens collimates the beam. The beam is then passed through the Hartmann sensor. The wedge pick-off shown in figure 3 was added before the sensor grid to allow the use of a Shack-Hartmann wavefront sensor in the system.

Using the spot images from the system itself as a reference, wavefront aberrations were introduced by adding optical elements (aberration sources shown in fig. 3) approximately 5 cm after the focus of the beam expander to disrupt the collimation. Plano-convex lenses were

used, with focal lengths of 200, 300, and 500 mm. By comparing the spot patterns of the system with and without these lenses, the additional wavefront error these lenses introduce can be measured.

3.1 Design Simulations

There are several key parameters for designing a Hartmann sensor. The number of apertures should be maximized within practical limits to ensure a thorough sampling of slope points and create wavefront images with acceptable resolution. However, the apertures themselves must be large enough to minimize diffractive effects. The spacing of the apertures also must be large enough to prevent interference patterns from obscuring the spot image on the image sensor. This spacing is also significant for wavefronts with a high degree of aberration since spots from different apertures can overlap or switch positions relative to the reference image if those apertures are not far enough apart. Machining capabilities for aperture size and spacing must also be taken into account for the final product sensor. To avoid delays getting the simple grids manufactured in metal, the sensors for these tests were created by printing the grid design onto transparency slides using a laser printer. Although not the ideal material to block out the undesired sections of light, the transparency sensors were able to produce completely adequate spot patterns.

The light sensor of the available camera was 15.2 mm square, so the Hartmann sensor grid was also designed with this shape and size. An aperture diameter of 0.0635 cm was selected as the minimum size. Since this diameter is over one thousand times larger than the 532 nm wavelength of light in use on the test setup, the effect of diffraction expected on the resulting image would be minimized. This allows a maximum of 23 apertures on each side of

the square grid. However, this configuration is not likely to result in a clear spot image since the spots will be too close and will blur together. Therefore, simulations were carried out to determine an aperture size and spacing capable of producing an acceptable image.

A MATLAB script was written to model several configurations of Hartmann sensors through which various wavefronts were propagated. The sensors were modeled using logical matrices. Spaces within the apertures of the sensor were given a value of one, while outside areas were set to zero. Figure 4 shows the logical matrix of the 19 by 19 grid eventually used in the experiment. Wavefronts could then be mathematically modeled and multiplied by the logical matrix in order to simulate which sections of a beam would pass through the sensor. Using a MATLAB function, FresnelPropagator [4], the patterns formed by propagating these zonal sections of the beam a specified distance were calculated and displayed. Figure 5(a) is a plot of the simulated spot pattern from the 19 by 19 Hartmann grid, propagated 250 mm from the grid. This simulation shows that the designed sensor can produce clear, acceptable images that a computer should be able to read and reconstruct, without confusing light from adjacent spots. The quality of the images was verified by running the simulated spot patterns through reconstruction code and seeing that the expected wavefront images of various simulated tilts and defocuses were obtained.

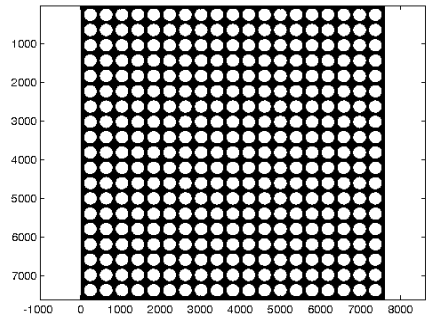

Figure 4: 19 by 19 Hartmann Sensor
This is a representation of the logical matrix used to model the Hartmann sensor used in the experiment. The axis scales represent the number of elements on each axis.

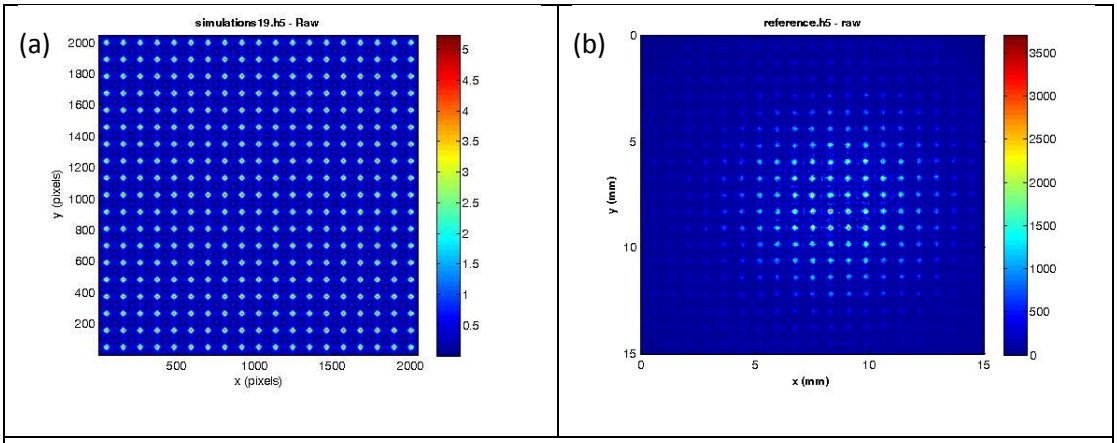

Figure 5: Simulated Spot Pattern of the 19 by 19 Sensor - The image (a) is a raw spot image resulting from the simulated propagation of an ideal plane wavefront, amended by the logical matrix in figure 4, a distance of 250 mm using the FresnelPropagator function. The spot pattern is clear and suitable for wavefront reconstruction. The experimental pattern using the same sensor design is shown in image (b).

Figure 5(b) shows the spot pattern attained using the designed sensor in the lab set-up. This experimental result agrees quite well with the simulated data. The simulation includes effects from diffraction, causing slight fringes to appear between the spots. The experimental diagram shows these effects as well. The clarity in size and spacing of the spots in the pattern is also consistent. The brightened central area on the experimental pattern is caused by the intensity profile of the experimental laser, which was brightest in the center and faded towards the sides of the beam.

4. Wavefront Measurements

Wavefront measurements were taken for the test laser system with each of the three aberration source lenses. These measurements were taken simultaneously using the Hartmann sensor being tested and the Shack-Hartmann sensor.

4.1 Hartmann Sensor

When examining wavefront images, it is common to remove tilt and power from the image in order to see lower-level and smaller features in the wavefront. Removing tilt fits a plane to the wavefront modeled h(x,y) and subtracts it off, eliminating effects that most often result from misalignment between the beam and the camera. Power is removed because, on an uncollimated beam, the wavefront errors from this aberration often overshadow higher-order aberrations. By fitting a paraboloid shape to the image and subtracting it out, aberrations such as coma and astigmatism become evident. Figure 6 shows all of these images from the three test lenses, as determined by the Hartmann sensor reconstructions.

Peak-to-valley (P-V) and root-mean-square (RMS) values were calculated for each image to provide statistics to compare with results from other wavefront sensors. The P-V measurement is most useful on the raw wavefront reconstructions and those with removed tilt, because it quantifies the amount of power or defocus on the beam. When this effect is removed, the RMS value becomes a more useful statistic since it measures the amount of variation about the mean distance and provides a measurement of the amount of higher-order aberration.

200 mm Lens	300 mm Lens	500 mm Lens
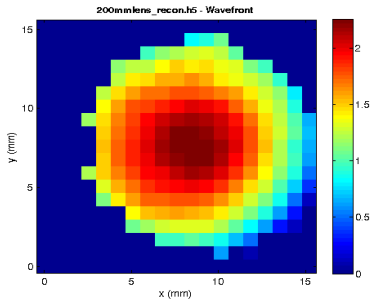	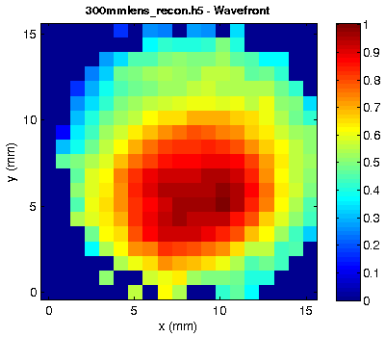	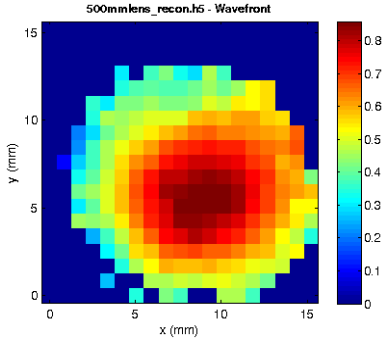
P-V = 2.2 wvs RMS = 0.5 wvs	P-V = 0.9 wvs RMS = 0.2 wvs	P-V = 0.9 wvs RMS = 0.3 wvs
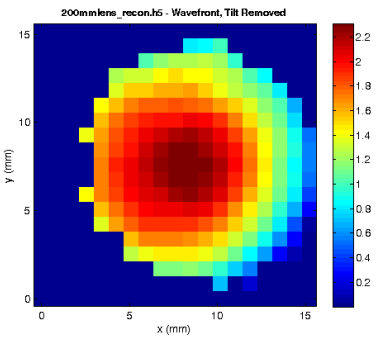	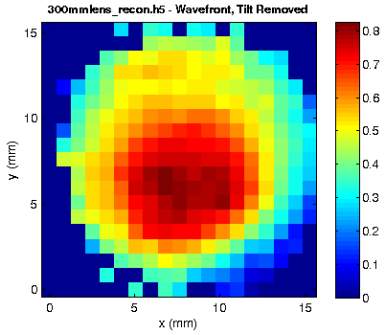	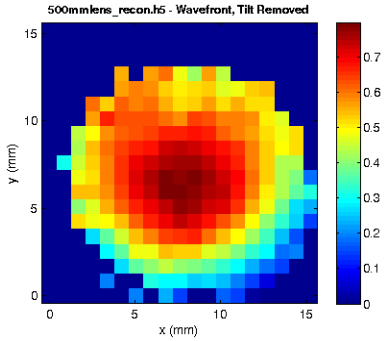
P-V = 2.2 wvs RMS = 0.5 wvs	P-V = 0.8 wvs RMS = 0.2 wvs	P-V = 0.8 wvs RMS = 0.3 wvs
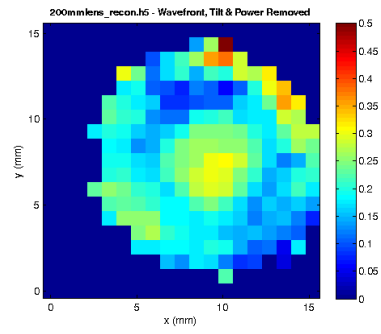	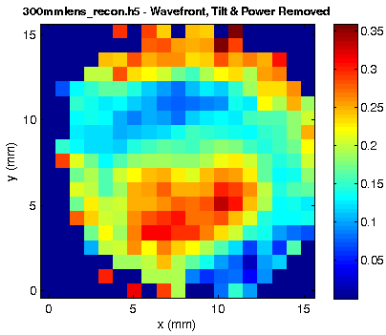	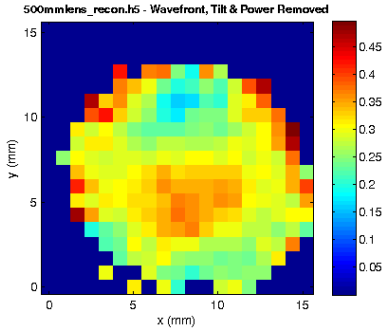
P-V = 0.5 wvs RMS = 0.1 wvs	P-V = 0.3 wvs RMS = 0.1 wvs	P-V = 0.5 wvs RMS = 0.2 wvs

Figure 6: Hartmann Sensor Wavefront Reconstructions – These diagrams show the wavefronts measured using each test lens. The top row shows raw wavefront images, the middle the same images with tilt removed, and the bottom the images with both tilt and power removed. When the defocus seen in the first two rows is removed, each image shows, to varying extents, coma, an aberration that resulted from slight lens misalignment.

In order to provide a reference to assess the accuracy of the reconstructed wavefront images, the system with the 500 mm test lens was modeled using a ray-tracing optical modeling program, OSLO [5]. The shape of each lens surface, the spacing of each surface, and the

material of each lens were entered into OSLO, and an expected wavefront measurement was calculated. The raw and tilt-removed wavefronts measured by the Hartmann sensor for the 500 mm lens in figure 6 show close agreement to the OSLO calculations in figure 7.

(a) Raw Image	(b) Tilt Removed
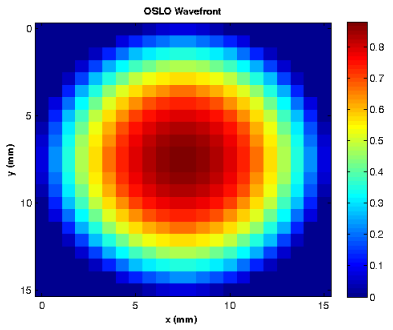	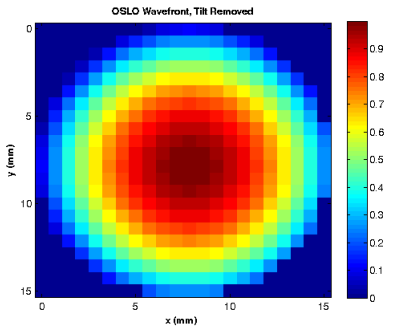
P-V = 0.9 wvs RMS = 0.3 wvs	P-V = 1.0 wvs RMS = 0.3 wvs

Figure 7: OSLO Wavefront Calculations for the 500 mm Test Lens – The amount of defocus predicted by OSLO shows excellent agreement with the corresponding experimental results in figure 6.

By adjusting the model distance parameters within setup and measurement uncertainties, the raw wavefront prediction and tilt-removed wavefront were found to be almost identical. When power was removed from the OSLO wavefront, a perfectly flat wavefront was measured. This occurred because OSLO assumed perfect lens alignment, and no significant higher-order aberration was introduced.

4.2 Shack-Hartmann Sensor

In order to further verify the results from the Hartmann sensor reconstructions, a commercial Shack-Hartmann sensor, a HASO3 128-GE, [6] was added to the optical system. Similar to the Hartmann sensor, this Shack-Hartmann sensor compares spot patterns to make wavefront measurements. However, the use of lenslets instead of empty apertures and a pre-programmed reference image on the Shack-Hartmann sensor distinguish the two techniques.

The Shack-Hartmann wavefronts showed the coma and other higher-order imperfections caused by human error in the alignment of the system, giving greater credibility to the Hartmann results. Figure 8 shows the Shack-Hartmann results comparable to the Hartmann data in figure 6.

Several factors impact the ability to make perfect comparisons between the Hartmann and Shack-Hartmann results. The Shack-Hartmann sensor imaged a reflection of the beam from a pick-off. An unwanted reflection from the second surface of the pick-off optic overlapped with part of the desired reflection, making it possible to measure only a section of the beam on the light sensor. This led to smaller peak-to-valley and root mean square values. By measuring the distance between the center of the beam image and the outer edge and assuming a perfect paraboloid shape (i.e. power dominates the wavefront shape), it is possible to scale the peak-to-valley value to account for the smaller P-V size of the beam and create an estimate of the measurement had the beam size been larger. Using this scaling technique, the wavefront statistics of the Hartmann and Shack-Hartmann sensor results show even closer agreement.

The scaling process is most accurate on the 500 mm lens, since it introduces the least power. The small difference between the tilt-removed Hartmann sensor P-V measurement with the 200 mm lens (2.2 wvs) and the corresponding Shack-Hartmann measurement (1.5 wvs) is likely because of the fact that power is not the only aberration in the wavefront.

200 mm Lens	300 mm Lens	500 mm Lens
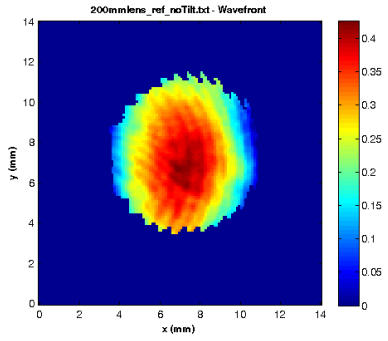	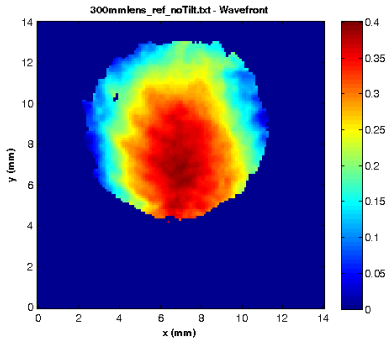	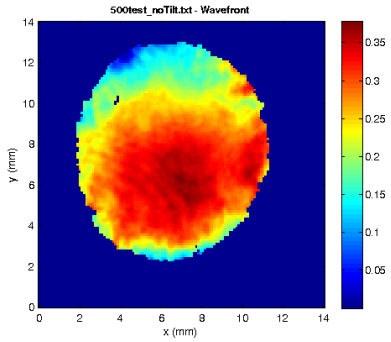
P-V = 0.4 wvs RMS = 0.1 wvs Scaled P-V = 1.4 wvs	P-V = 0.4 wvs RMS = 0.1 wvs Scaled P-V = 1.3 wvs	P-V = 0.4 wvs RMS = 0.1 wvs Scaled P-V = 0.7 wvs
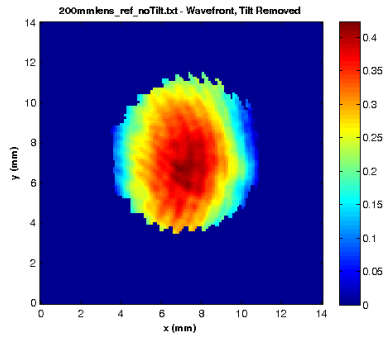	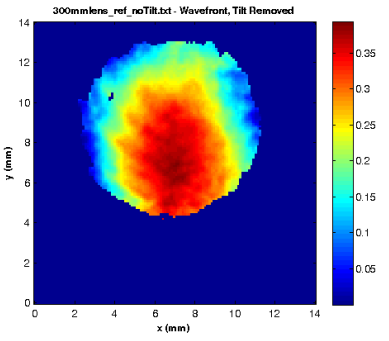	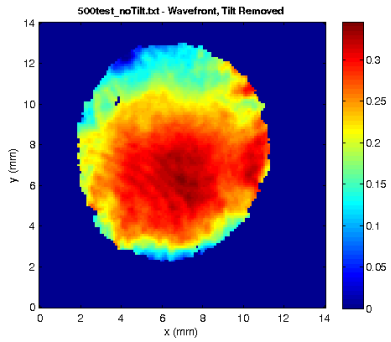
P-V = 0.4 wvs RMS = 0.1 wvs Scaled P-V = 1.5 wvs	P-V = 0.4 wvs RMS = 0.1 wvs Scaled P-V = 1.0 wvs	P-V = 0.3 wvs RMS = 0.1 wvs Scaled P-V = 0.5 wvs
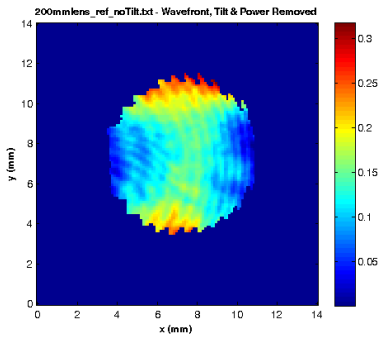	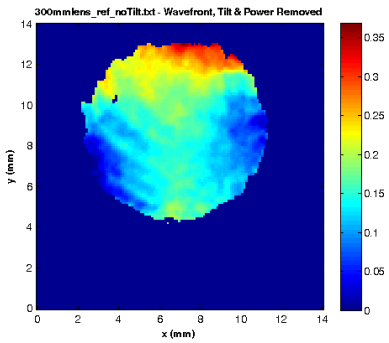	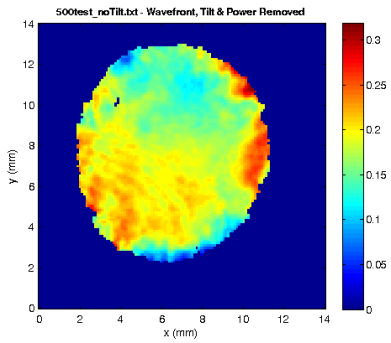
P-V = 0.3 wvs RMS = 0.0 wvs	P-V = 0.4 wvs RMS = 0.1 wvs	P-V = 0.3 wvs RMS = 0.1 wvs

Figure 8: Shack-Hartmann Sensor Wavefront Reconstructions – This figure shows the Shack-Hartmann reconstructions corresponding to the Hartmann wavefronts in figure 6. Raw wavefront measurements and those with tilt removed have scaled peak-to-valley values using the technique discussed in the text. The interference fringing visible on several of the images is due to the overlap of the secondary reflection from the opposite side of the wedged pick-off.

Referencing the Shack-Hartmann images also adds differences between the Shack-Hartmann and Hartmann measurements. Since the reference image for the Hartmann sensor includes minor errors in the collimated system, these aberrations do not appear in the reconstructions. Although a shear plate was used to check the collimation, some error remained present in the optical system. The Shack-Hartmann sensor uses software with a pre-made factory reference pattern, and so does not account for the aberration of the system. In order to remove these effects from the Shack-Hartmann image, a wavefront measurement of the system itself was made and subtracted from the later measurements. Since adding the aberration sources affected the pointing and size of the beam, this manual referencing process was not completely accurate in the removal of system aberrations. These referencing and size errors can account for the discrepancy between the Shack-Hartmann and the Hartmann measurements, which still show excellent agreement.

5. Conclusions

The ability to use Hartmann sensors would be valuable to the OMEGA EP system because it would allow wavefront diagnosis in UV portions of the system, something that is not currently feasible. A simply manufactured Hartmann sensor was tested and proven to have acceptable accuracy in a small system. MATLAB code was used to determine an aperture size and spacing to create legible spot patterns. Comparison between the experimental results from the designed Hartmann sensor and those from a Shack-Hartmann sensor confirmed the Hartmann sensor's accuracy. Hartmann sensing techniques have therefore been proven to be effective and suitable for implementation on the OMEGA EP laser system.

It will benefit OMEGA EP in several ways to incorporate the use of Hartmann sensors. Ultraviolet portions of the system would be diagnosable, as would the UV probe beam used for plasma interferometry. Since the interferometry results are affected by wavefront aberrations, a measurement of the beam prior to passing through the plasma would be a useful diagnostic. On the larger system, UV wavefront measurements would provide information on wavefront aberrations introduced by the final IR optics and the wavefront shape before entering the target chamber. Knowing these measurements will also help determine the area the beam covers on the final UV optics, allowing a calculation of energy intensity there, a current limiting factor for the beam entering the target chamber. Taking measurements with a Hartmann sensor will aid in the adjustment of optics to reduce wavefront aberration, ultimately allowing an increase in the energy output of the system.

6. Acknowledgements

I would like to thank my advisor, Dr. Matthew Barczys, for giving me the opportunity to work on this project and his constant support throughout the summer. Dr. Brian Kruschwitz's assistance was invaluable in creating the simulation code. Parts of the wavefront reconstruction code were written by Dr. Seung-Whan Bahk, and I greatly appreciate this contribution to the project. Finally, I owe gratitude to the Laboratory for Laser Energetics and all who are involved there, and especially to Dr. Craxton for offering me this opportunity.

7. References

[1]. J. H. Kelly, L. J. Waxer, V. Bagnoud, I. A. Begishev, J. Bromage, B. E. Kruschwitz, T. J. Kessler, S. J. Loucks, D. N. Maywar, R. L. McCrory, D. D. Meyerhofer, S.F. B. Morse, J. B. Oliver, A. L. Rigatti, A. W. Schmid, C. Stoeckl, S. Dalton, L. Folnsbee,

M. J. Guardalben, R. Jungquist, J. Puth, M. J. Shoup III, D. Weiner, and J. D. Zuegel. “OMEGA EP: High-Energy Petawatt Capability for the OMEGA Lase Facility,” J. Phys. IV France 133, 75 (2006).

[2]. Daniel Malacara, ed., Optical Shop Testing (J. Wiley and Sons, New York, 1978).

[3]. D. H. Froula, R. Boni, M. Bedzyk, R. S. Craxton, F. Ehrne, S. Ivancic, R. Jungquist, M.J. Shoup, W. Theobald, D. Weiner, N.L. Kugland, and M.C. Rushford. Optical diagnostic suite (schlieren, interferometry, and grid image refractometry) on OMEGA EP using a 10-ps, 263-nm probe beam. Rev. Sci. Instrum. 83, 10E523 (2012).

[4]. B. E. Kruschwitz, Unpublished, 2012.

[5]. Optics Software for Layout and Optimization [Software]. (2009). Littleton, MA: Lambda Research Corporation.

[6]. Prosilica GE2040, Allied Vision Technologies.